ACS APPLIED MATERIALS & INTERFACES

Research Article

www.acsami.org

Enhanced Gas Sensing Performance of Electrospun Pt-Functionalized NiO Nanotubes with Chemical and Electronic Sensitization

Jiecai Fu,* Changhui Zhao, Junli Zhang, Yong Peng, and Erqing Xie*

Key Laboratory of Magnetism and Magnetic Materials of Ministry of Education, Lanzhou University, Lanzhou 730000, P. R. China

Supporting Information

ABSTRACT: Pt-functionalized NiO composite nanotubes were synthesized by a simple electrospinning method, and their morphology, chemistry, and crystal structure have been characterized at the nanoscale. It was found that the Pt nanoparticles were dispersed uniformly in the NiO nanotubes, and the Pt-functionalized NiO composite nanotubes showed some dendritic structure in the body of nanotubes just like thorns growing in the nanotubes. Compared with the pristine NiO nanotube based gas sensor and other NiO-based gas sensors reported previously, the Pt-functionalized NiO composite nanotube based gas sensor showed substantially enhanced electrical responses to target gas (methane, hydrogen, acetone, and ethanol), especially ethanol. The NiO−Pt 0.7% composite nanotube based gas sensor displayed a response value of 20.85 at 100 ppm at ethanol and 200 °C, whereas the pristine NiO nanotube based gas sensor only showed a response of 2.06 under the same conditions. Moreover, the Pt-functionalized NiO composite nanotube based gas sensor demonstrated outstanding gas selectivity for ethanol against methane, hydrogen, and acetone. The reason for which the Pt-functionalized NiO composite nanotube based gas sensor obviously enhanced the gas sensing performance is attributed to the role of Pt on the chemical sensitization (catalytic oxidation) of target gases and the electronic sensitization (Fermi-level shifting) of NiO.

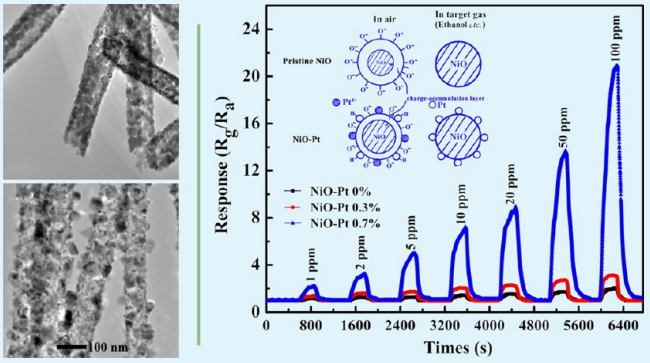

KEYWORDS: *pristine NiO, Pt-functionalized NiO, chemical sensitization, electronic interaction, electronic sensitization, Fermi-level shifting*

1. INTRODUCTION

Solid-state gas sensors made by oxide semiconductors have been subjected to extensive research since they were first proposed in 1962, and they have now widely developed into an important functional field for detecting the leakage of several kinds of inflammable gases and some toxic gases.[1−4] In practical applications, these gases often exist at a very low level or under a hostile condition so that relevant gas sensor devices should be designed for the detection of the danger. To meet such low-level gases and hostile conditions, the sensors should be highly upgraded in sensitivity and selectivity. So far, the sensing properties of various kinds of materials, such as SnO_2, ZnO, WO_3, and In_2O_3, have been studied.[5−8] However, those studies always show either unsatisfying sensitivity or poor selectivity. Therefore, it is urgent to find a way to fabricate gas sensing materials with high sensitivity and outstanding selectivity.

It is known that two important aspects of sensor elements are involved in the response of gas sensors, including recognition by the reactive surface and transducing by a sensing layer.[9] In air, the oxygen adsorbed on the oxide traps conduction electrons and then induces an electron-depleted (or charge-accumulated) space charge layer at the surface of the oxide nanograin. Upon exposure to the target gas, the adsorbed oxygen was consumed, resulting in a decrease of space-charge-layer thickness, which brings about the resistance changes ultimately. Therefore, the improvement of recognition and transducing would be a good way to improve the sensing performance of gas sensors. Hollow and porous nanofibers are promising sensing platforms to enhance gas sensing performance because both inner and outer surfaces of nanofibers can participate in the gas sensing reaction. Furthermore, in the hollow and porous configuration, the introduction of a foreign material or element which is very reactive to the target gas would make it possible to obtain an ideal gas sensor with high sensitivity and outstanding selectivity.[10−13] Although the addition of these materials has been known to be effective in promoting gas sensitivity under certain conditions, the mechanism of these sensitization effects has not been well understood.

As an important member of the semiconductor oxide family for gas sensors, nickel oxide (NiO) has attracted extensive investigation due to its significant qualities such as the relative wide band gap (E_g = 3.6−4.0 eV), relatively considerable electrical conductivity change along with chemical reactions on

Received: May 8, 2013
Accepted: July 11, 2013
Published: July 11, 2013

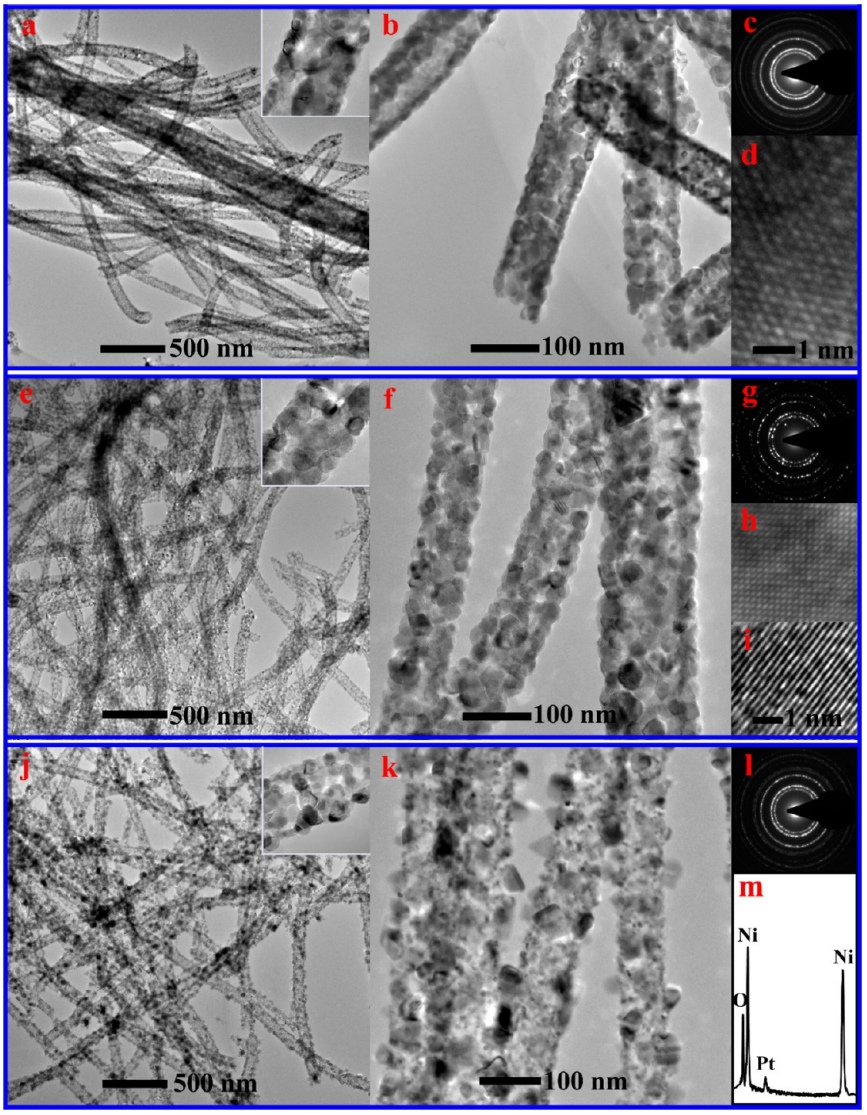

Figure 1. Morphologies and crystal structures of pristine NiO, NiO−Pt 0.3%, and NiO−Pt 0.7% nanotubes: (a−d) characterization of NiO nanotubes via low-, high-magnified TEM images (a, b), a SAED pattern (c), and lattice fringe image of the NiO nanoparticle included in the nanotubes (d); (e−i) characterization of NiO−Pt 0.3% nanotubes via low-, high-magnified TEM images (e, f), a SAED pattern (g), and lattice fringe images of the Pt nanoparticle (h) and NiO nanoparticle (i) included in the nanotubes; (j−m) characterization of NiO−Pt 0.7% nanotubes via low-, high-magnified TEM images (j, k), a SAED pattern (l), and an EDX spectrum (m).

the surface of materials, etc., all making it a good candidate for gas sensor applications.[14,15] Nevertheless, finding a way to realize large-scale and cost-effective production of high-quality freestanding one-dimensional NiO nanomaterials is still a gap needing bridge. Among various fabrication methods, electrospinning is believed to satisfy the requirements. It is a process by which very fine fibers (with a diameter on the micro- or nanoscale and lengths up to kilometers) are drawn from a liquid by an electrical charge.[16] It has been widely adopted to prepare various 1D nanomaterials with several kinds of nanostructures because of simplicity, low cost, relatively high production rate, and easy doping for obtaining composite nanomaterials.[17−19]

In this work, we present an investigation on the fabrication and gas sensing properties of pristine NiO and Pt-functionalized NiO nanotubes prepared by the electrospinning method. The morphology and structure and chemical and gas sensing properties have been systemically investigated. Moreover, prototype gas sensors using NiO and Pt-functionalized NiO nanotubes have been fabricated and their sensing mechanisms have been explored.

2. EXPERIMENTAL SECTION

2.1. Fabrication of Pristine NiO and NiO−Pt Nanotubes. To synthesize NiO and NiO−Pt nanotubes, a two-step process was adapted as described below. In the first step, 0.35 mmol of nickel nitrate hexahydrate ($Ni(NO_3)_2{\cdot}6H_2O$, A.R., Alfa-Aesar Inc., USA) and polyvinylpyrrolidone (PVP, $M_w \approx 1\,300\,000$, Sigma-Aldrich Inc., USA) were dissolved in a mixed solution of 1.25 mL of *N*,*N*-dimethyl formamide (DMF, A.R., Tianjin Chemical Corp., China) and 1.25 mL of ethanol (A.R., Tianjin Chemical Corp., China). Subsequently, to obtain Pt-doped NiO−Pt nanotube, chloroplatinic acid (H_2PtCl_6, A.R., Alfa-Aesar Inc., USA) was added into the above PVP/$Ni(NO_3)_2$ solution, and the molar ratio of H_2PtCl_6:$Ni(NO_3)_2$ ranged from 0.1:99.9 to 0.9:99.1. After vigorous magnetic stirring overnight, the viscous gel of PVP/$Ni(NO_3)_2$−H_2PtCl_6 composite was transferred into a glass syringe equipped with a 5# stainless needle whose inner diameter was about 0.34 mm. The needle was connected to a high-voltage generator (ES30P-5W, Gamma High Voltage Research Inc.,

dx.doi.org/10.1021/am4017347 | ACS Appl. Mater. Interfaces 2013, 5, 7410−7416

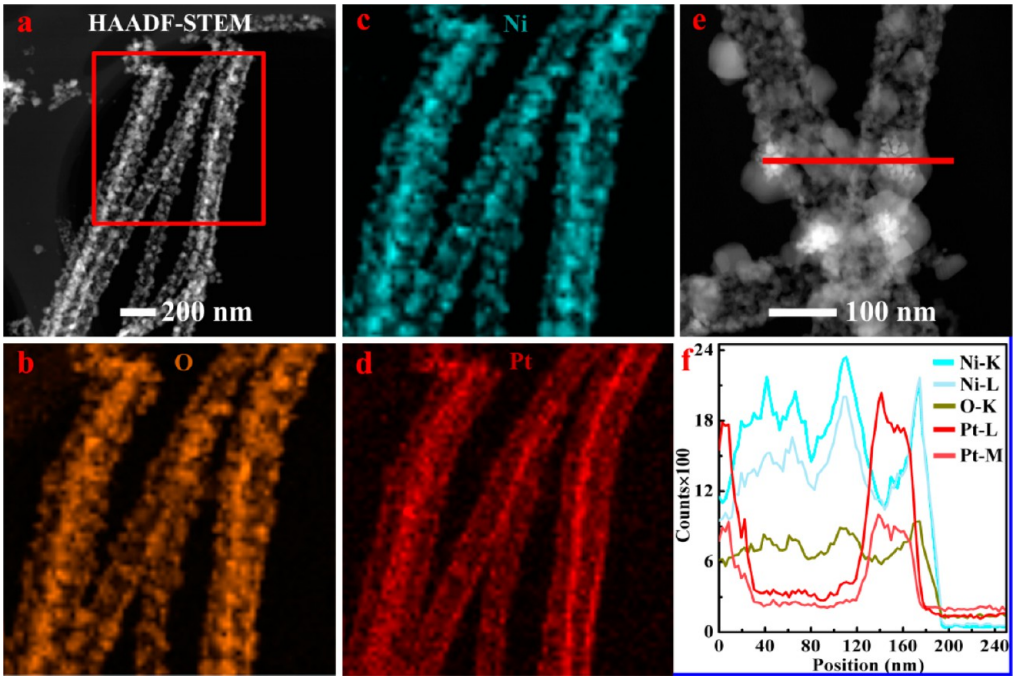

Figure 2. (a–d) EDX mappings of individual NiO–Pt 0.7% nanotubes: representative STEM-HAADF image (a), oxygen mapping (b), nickel mapping (c), platinum mapping (d); (e) STEM-HAADF image of two crossed NiO–Pt 0.7% nanotubes showing the branched structure; (f) line-scan profiles of Ni, O, and Pt elemental distribution in the selected area indicated in the corresponding HAADF-STEM image (marked by a red line in part e).

USA) which is capable of generating DC voltages up to 30 kV. In this case, a voltage of 12 kV was applied between the cathode (a metal collector) and the anode (needle) with the spacing of 15 cm. And the viscous gel was continuously supplied using a syringe pump (LSP01-1A, Baoding Longer syringe pump Corp., China) at a rate of 0.25 $mL \cdot h^{-1}$.

After electrospinning, the electrospun polymer composite nanofibers were collected and annealed in the air at 200 °C with a heating rate of 1 $°C \cdot min^{-1}$, and then sintered at 500 °C for 2 h. To obtain good crystalline quality, the sample was permitted to cool down to room temperature at a rate of 2 $°C \cdot min^{-1}$.

2.2. Fabrication and Testing of Gas Sensors. The synthesized nanotubes were mixed with terpineol in a weight ratio of 80:20 to form a paste. The paste was deposited on alumina-ceramic tubes with a pair of gold electrodes by the dip-coating method to form a sensing layer (250–300 μm in thickness), and then dried at 80 °C for 3 h. Finally, the ceramic tubes were connected to a Bakelite base and a Ni–Cr heating wire was inserted into the tube to form a side-heated gas sensor, as illustrated in Figure S1 (see the Supporting Information).

The gas sensing properties of the sensor were measured by using a static test system (WS-30A, Winsen Electronics Co. Ltd., China). A certain volume of target gas was injected into the test chamber (18 L in volume) by a microinjector and mixed with air (the relative humidity was below 30%) by two fans in the test chamber, and clean air was used as a reference gas. The sensor response (S_r) was defined as the ratio of the sensor resistance in target gases (R_g) to that of in dry air (R_a), which was measured at a temperature ranging from 160 to 300 °C.

2.3. Characterization. The morphologies of the NiO and NiO–Pt nanotubes were characterized by a high resolution transmission electron microscope (HRTEM, Tecnai G^2 F30, FEI, USA) equipped with an energy-dispersive X-ray analyzer (EDAX, AMETEK Co., Ltd., USA) and a high angle annular dark field-scanning transmission electron microscope (HAADF-STEM). The X-ray diffraction (XRD, Philips X'pert Pro MPD (Cu Kα radiation), The Netherlands) instrument was employed to study the crystallographic properties. X-ray photoelectron spectroscopy (XPS) measurements were carried out on a spectrometer (ESCALAB210, VG, UK) using Mg Kα radiation (1253.6 eV) at room temperature under 3×10^{-8} Torr.

3. RESULTS AND DISCUSSION

3.1. Morphologies and Chemical Analysis. Morphologies and crystal structures of the pristine NiO, NiO–Pt 0.3%, and NiO–Pt 0.7% nanotubes were observed by TEM. Figure 1a represents a typical TEM image of NiO nanotubes, revealing a continuous structure and virtually uniform diameter (~80 nm) after the PVP was burned off. Each NiO nanotube is composed of a number of NiO single nanocrystallites (average grain size ~20 nm). These nanoscale single crystallites are stacked one by one along the direction of the nanotube axis, which is also demonstrated by the inset of Figure 1a, b, and d. The selected-area electron diffraction (SAED) pattern (Figure 1c) reveals that the NiO nanotube has a polycrystalline structure. Figure 1e and f exhibit two TEM images of NiO–Pt 0.3% composite nanotubes, revealing a morphology similar to that of a pure NiO nanotube except there are some tiny particles dispersed in the bodies of individual nanotubes. Lattice-resolution TEM images (Figure 1h and i) demonstrate that the NiO–Pt 0.3% composite nanotubes consist of Pt and NiO nanoparticles, with spacing distances matched with Pt(111) planes and NiO(200) planes, respectively. This result is consistent with the SAED results shown in Figure 1g. Figure 1j shows a low-magnified TEM image of the NiO–Pt 0.7% composite nanotubes, of which quantitative analysis reveals an 85 nm average diameter. The high-magnified TEM image (Figure 1k) reveals that the morphology of the NiO–Pt 0.7% composite nanotubes is clearly different from that of the above NiO (Figure 1b) and NiO–Pt 0.3% (Figure 1f) nanotubes. Individual NiO–Pt 0.7% composite nanotubes appear to have a dendritic structure in the body of nanotubes just like thorns growing in the nanotubes, and the size of individual thorns

dx.doi.org/10.1021/am4017347 | ACS Appl. Mater. Interfaces 2013, 5, 7410–7416

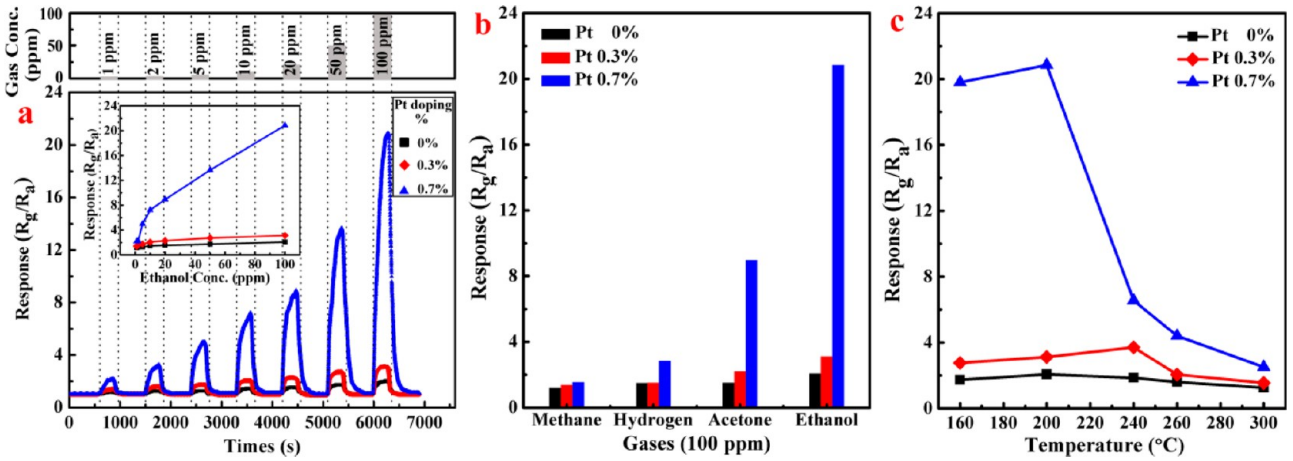

Figure 3. (a) Response and recovery characteristic curve of the NiO, NiO−Pt 0.3%, and NiO−Pt 0.7% nanotube based gas sensors to ethanol in the range 1−100 ppm at 200 °C; the inset shows the response versus ethanol concentration for the three gas sensors. (b) The response selectivity of the three sensors for the gases (methane, hydrogen, acetone, and ethanol) at a concentration of 100 ppm at 200 °C. (c) Dependence of ethanol response on operating temperature at a gas concentration of 100 ppm.

(~20 nm) is bigger than that of NiO particles (~8 nm). It is also seen that some tiny particles uniformly dispersed through each integral nanotube, which were Pt nanoparticles as proven below. The EDX spectrum (Figure 1m) collected from a bunch of NiO−Pt 0.7% composite nanotubes shows that the main elements are Ni, O, and Pt. The SAED in Figure 1l reveal that the NiO nanotubes are polycrystalline with a rock-salt structure, the same as the above NiO and NiO−Pt 0.3% nanotubes. The reason is believed to derive from the low concentration and phase separation of the Pt element.

To preliminarily understand the distribution of NiO−Pt composite nanotubes, the detailed chemical elemental distribution of individual NiO−Pt 0.7% composite nanotubes was further studied by EDX mapping and EDX line scanning techniques (Figure 2) on a 300 kV HRTEM. Figure 2a shows a representative HADDF-STEM image of a bunch of NiO−Pt 0.7% composite nanotubes, clearly revealing a thorn-adjoining-nanotube-like morphology. This observation is consistent with the above TEM finding, but showing much clearer and better spatial resolution. Parts b−d of Figure 2 show the corresponding EDX elemental mappings of oxygen, nickel, and platinum elements, respectively. It is seen that elements O, Ni, and Pt, as detected by K-shell X-ray or L-shell X-ray, are evenly distributed throughout each nanotube, revealing that the NiO formed a uniform chemical phase and the Pt nanoparticles are homogeneously dispersed in the nanotubes with a relatively smaller size. Figure 2e shows another HADDF-STEM image of individual NiO−Pt 0.7% composite nanotubes. The contrast of incoherent high-resolution HADDF-STEM images depends directly on the sample atomic number Z and thickness of the materials; in the composite nanotube image, a porous network phase composed of NiO and Pt nanoparticles is revealed, and the thorn-like dendritic structure in the nanotube body is NiO nanoparticles with bigger size than Pt nanoparticles and some of the Pt nanoparticles show a flower-like morphology, which can be seen more clear in highly magnified HADDF-STEM images (see the Supporting Information, Figure S2). Further line-scan profiles (Figure 2f) of Ni, O, and Pt elements in the selected area (marked by a red line in Figure 2e) indicate that the thorn-like dendritic structure is a core-Pt/shell-NiO structure.

3.2. Gas Sensing Performance Testing. In order to understand the role of catalytic Pt on NiO nanotubes and demonstrate the potential applications of Pt-functionalized NiO nanotubes in highly sensitive and selective gas sensors, gas responses (methane, hydrogen, acetone, and ethanol) of NiO, NiO−Pt 0.3%, and NiO−Pt 0.7% composite nanotube based gas sensors were measured, respectively. Figure 2a displays that the typical response and recovery characteristics of the three sensors exposed to ethanol gas ranging from 1 to 100 ppm at 200 °C. It can be seen that their gas responses increase with the increase of ethanol concentrations and Pt content. The NiO nanotube based sensor shows responses of approximately 1.16, 1.25, 1.27, 1.45, 1.54, 1.73, and 2.06 at 1, 2, 5, 10, 20, 50, and 100 ppm ethanol, respectively. In comparison, the NiO−Pt 0.7% composite nanotube based sensor shows responses of 2.17, 2.24, 4.97, 7.22, 8.92, 13.65, and 20.85 at the same ethanol concentrations, respectively (Table S1, Supporting Information, summarized from Figure 3a). It is seen that the sensing responses of the NiO nanotubes after doping with Pt nanoparticles have been improved approximately 2-, 2-, 4-, 5-, 6-, 8-, and 10-fold at 1, 2, 5, 10, 20, 50, and 100 ppm ethanol, respectively. In particular, the responses of the NiO−Pt 0.7% composite nanotube gas sensor tends to dramatically increase with the increase of ethanol concentration.

The responses of the NiO, NiO−Pt 0.3%, and NiO−Pt 0.7% nanotube based gas sensors to four target gases (methane, hydrogen, acetone, and ethanol) with 100 ppm concentration at operating temperatures of 200 °C were further investigated, and the relevant results are shown in Figure 3b. It is seen that these sensors were not sensitive for detecting methane and hydrogen but have good responses for detecting acetone and ethanol. In particular, the response of the NiO sensor to acetone and ethanol is relatively lower than that of the NiO−Pt 0.7% sensor, and the maximum response is 1.52, 2.06 for the NiO sensor and 8.97, 20.85 for the NiO−Pt 0.7% sensor, respectively. In a word, the Pt-functionalized NiO nanotube is more sensitive to ethanol than the other three target gases.

In addition, the dependence of ethanol response on operating temperature at a gas concentration of 100 ppm for the NiO, NiO−Pt 0.3%, and NiO−Pt 0.7% nanotube based sensors was studied, as shown in Figure 3c. It can be found that the response of the sensor increases with the increase of the

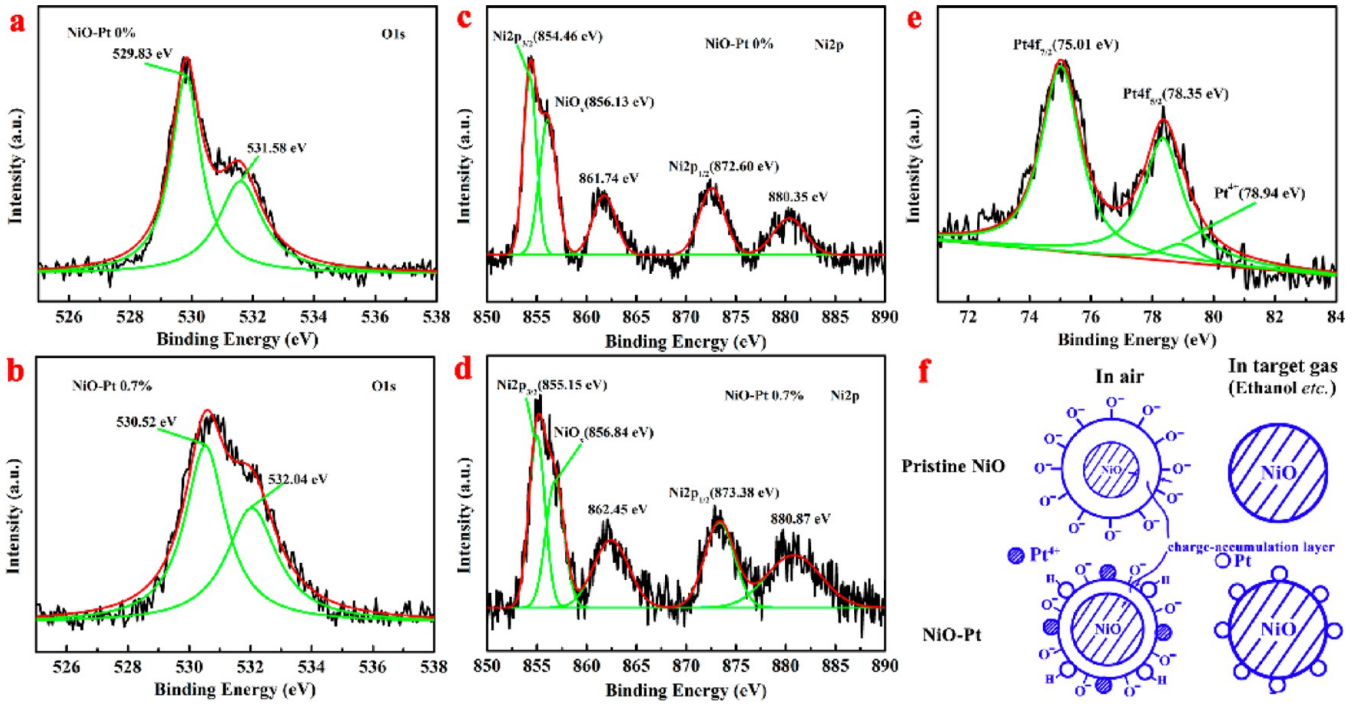

Figure 4. (a–e) XPS fine spectra of the pristine NiO nanotubes and NiO–Pt composite nanotubes: O 1s (a) and Ni 2p (c) in pristine NiO nanotubes; O 1s (b), Ni 2p (d), and Pt 4f (e) in the NiO–Pt composite nanotubes. (f) Schematic illustrating the mechanism of chemical and electronic sensitization in the pristine NiO elements (upper) and in the NiO–Pt elements (lower).

operating temperature in the beginning and reaches a maximum value at an optimal temperature (named optimum operating temperature), and then decreases with further increase of the operation temperature. It is worth noting that the optimum operating temperature decreases with the Pt content, and the optimum operating temperature for the NiO–Pt 0.7% nanotube based sensors is around 200 °C, which is lower than that of reported NiO.[10]

3.3. Mechanism of the Enhanced Gas Sensing Performance. It is known that gas sensing properties of metal oxides depend on several processes including surface adsorption and desorption and diffusion of gases in a porous membrane and inside a crystal lattice.[20] Therefore, the sensitivity and selectivity of gas sensors depend on the morphology and the nature of the sensor materials. In our case, the mechanism of enhanced gas sensing performance using Pt-functionlized NiO composite nanotubes can be depicted as follows.

In air, the oxygen adsorbed on the NiO trapped conduction electrons of the oxide and thus induced a charge-accumulation space charge layer at the surfaces of NiO nanograins. Upon exposure to the target gas (reducing gases), the adsorbed oxygen was consumed, resulting in a decrease in the space charge layer and thickness of the space charge layer. The absorbed oxygen worked as a sort of acceptor to target gas, and the relaxation in the space charge brought about a resistance change. The noble-metal-functionlization method has been reported to promote the gas sensing performance.[21,22] However, the way in which the surface function influences the gas response characteristics is still a subject of debate, and two mechanisms including the spillover and the Fermi-level mechanism are currently considered.[12,21]

To further confirm the mechanism of the enhanced sensing performance, the surface state of the pristine NiO and Pt–NiO system was investigated by XPS. Three freshly prepared samples, pristine NiO nanotubes, NiO–Pt 0.3%, and NiO–Pt 0.7% composite nanotubes, were examined and compared in their changes of surface state, as shown in Figure S3, Figure S4 (see the Supporting Information), and Figure 4. Figure S3 (Supporting Information) shows the XPS survey spectrum of the pristine NiO nanotubes and NiO–Pt 0.7% composite nanotubes, which indicates the existence of Pt in the NiO–Pt 0.7% composite nanotubes. Comparing the electron binding energies (BEs) of the pristine NiO nanotubes with those of NiO–Pt 0.7% composite nanotubes, it is found that the BEs of the NiO–Pt 0.3% elements and NiO–Pt 0.7% elements were bigger by about 0.3 and 0.8 eV than those of the pristine NiO, respectively, as shown in the fine spectra (Figure 4a–d and Figure S4, Supporting Information). These BE shifts are deduced to be intimately related to the chemical state of Pt. The dopant of catalytic Pt causes an upward shift of Ni and O signals from the levels of pristine NiO. In the Pt–NiO system, the Pt is dispersed as fine particles on the surface of each NiO naoparticle. Direct evidence from the deconvolution of Pt 4f in NiO–Pt elements shows the existence of $Pt(OH)_2 \cdot nH_2O$ (Figure 4e). Therefore, it is believed that an electronic interaction between the Pt and NiO surfaces would occur and these BE shifts originate from this electronic interaction (also named electronic sensitization), which increases the Fermi level of NiO or decreases the work function of NiO.

To figure out the mechanism of electronic sensitization in the pristine NiO elements (upper) and in the NiO–Pt elements (lower), a possible schematic is illustrated in Figures 4f and 5. The promoter (Pt) has an electronic sensitization role during the sensing process. When exposed to air, each Pt nanoparticle consisting of Pt and Pt^{4+} forms a redox electrode Pt^{4+}/Pt^0. To attain electronic equilibrium with the Pt nanoparticles, the Fermi level (E_F) of NiO will be shifted and

dx.doi.org/10.1021/am4017347 | ACS Appl. Mater. Interfaces 2013, 5, 7410–7416

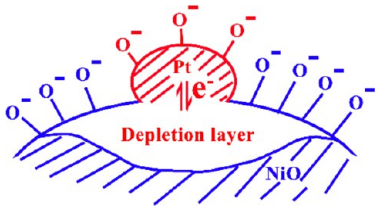

Figure 5. Schematic model of the electronic interaction between Pt and NiO.

pinned at the Pt^{4+}/Pt^0 electrode potential, which produces an electron depleted space charge region and decreases the charge-accumulation space charge layer (as illustrated in Figure 5). This eventually leads to an increase of resistance in air of the pristine NiO, NiO−Pt 0.3%, and NiO−Pt 0.7% nanotube based sensing layers at 200 °C (see the Supporting Information, Figure S5). Then, the oxidation state of the promoter is reduced to metal (Pt) when the NiO−Pt system is exposed to the target gas, while the electronic interaction is ruptured which accompanies the change of the electronic state of NiO accordingly.

In addition, it should be noted that the functionalized Pt nanoparticles also play an important role for promoting the gas sensing reaction by the spillover effect, which has been widely reported in previous literatures and is rather familiar in catalytic chemistry. The Pt nanoparticles in this case activate the target gas species to facilitate its catalytic oxidation on the NiO nanograin surface, as illustrated in Figure 4f. During the sensing process, the target gas species (e.g., ethanol) decomposition reaction on the surface of the NiO can be expressed as

$$C_2H_5OH + O_{ads}^-/O_2^- \rightarrow C_2H_4O + H_2O + e^-$$

$$C_2H_4O + O_{ads}^-/O_2^- \rightarrow CO_2 + H_2O + e^-$$

The Pt nanoparticle increases the gas sensitivity as it increases the rate of the chemical processes, leading to a decrease in concentration of the negatively charged adsorbed oxygen and resulting in a decrease of the space charge layer and thickness of the space charge layer. In combination with the porous structure of the prepared nanotubes, either the pristine NiO or NiO−Pt composite nanotubes, the target gases can elongate the retention time on the surface of NiO nanograins.

4. CONCLUSIONS

In conclusion, Pt-functionalized NiO composite nanotubes were synthesized via electrospinning. Different loading contents of Pt were carefully controlled by adding chloroplatinic acid. The Pt nanoparticles uniformly dispersed in the nanotubes and the Pt-functionalized NiO composite nanotubes appeared as some dendritic structure in the body of nanotubes just like thorns growing in the nanotubes. Compared with the pristine NiO nanotube gas sensor and reported NiO-based gas sensor, the Pt-functionalized NiO composite nanotube based gas sensor showed substantially enhanced responses to target gas (methane, hydrogen, acetone, and ethanol), especially ethanol. The gas response of the NiO−Pt 0.7% composite nanotube based gas sensor to 100 ppm ethanol was about 10-fold higher than that of the pristine NiO nanotubes. Moreover, remarkably high selectivity for ethanol against methane, hydrogen, and acetone gases was observed in the NiO−Pt 0.7% composite nanotube based gas sensor. Considerably more active site and leveling of Fermi level were found at the Pt-functionalized NiO nanotubes in comparison with the pristine NiO nanotubes during the adsorption or desorption of target gaseous species. It is believed that this work will open a new route to investigate the interaction between additives and semiconductor oxides so as to improve the sensing performance of gas sensors.

■ ASSOCIATED CONTENT

Supporting Information

Additional method information, schemes, SEM image, response table, and XPS spectrum. This material is available free of charge via the Internet at http://pubs.acs.org.

■ AUTHOR INFORMATION

Corresponding Author

*E-mail: fujc06@gmail.com (J.F.); xieeq@lzu.edu.cn (E.X.). Phone: +86 (0) 931 891 2425. Fax: +86 (0) 931 891 4160.

Notes

The authors declare no competing financial interest.

■ ACKNOWLEDGMENTS

This work was supported by the Natural Science Foundation of China (Grant No. 61176058), Chinese Academy of Sciences Joint Fund of Research Utilizing Large-scale Scientific Facilities (Grant No. U1232121), and the Scholarship Award for Excellent Doctoral Student granted by Lanzhou University.

■ REFERENCES

(1) Seiyama, T.; Kato, A.; Fujiishi, K.; Nagatani, M. *Anal. Chem.* **1962**, *34*, 1502−1503.
(2) Sysoev, V. V.; Goschnick, J.; Schneider, T.; Strelcov, E.; Kolmakov, A. *Nano Lett.* **2007**, *7*, 3182−3188.
(3) Kong, J.; Franklin, N. R.; Zhou, C.; Chapline, M. G.; Peng, S.; Cho, K.; Dai, H. *Science* **2000**, *287*, 622−625.
(4) An, K. H.; Jeong, S. Y.; Hwang, H. R.; Lee, Y. H. *Adv. Mater.* **2004**, *16*, 1005−1009.
(5) Zhang, Y.; He, X.; Li, J.; Miao, Z.; Huang, F. *Sens. Actuators, B* **2008**, *132*, 67−73.
(6) Ahn, M. W.; Park, K. S.; Heo, J. H.; Park, J. G.; Kim, D. W.; Choi, K. J.; Lee, J. H.; Hong, S. H. *Appl. Phys. Lett.* **2008**, *93*, 263103.
(7) Ponzoni, A.; Comini, E.; Sberveglieri, G.; Zhou, J.; Deng, S. Z.; Xu, N. S.; Ding, Y.; Wang, Z. L. *Appl. Phys. Lett.* **2006**, *88*, 203101.
(8) Waitz, T.; Wagner, T.; Sauerwald, T.; Kohl, C.-D.; Tiemann, M. *Adv. Funct. Mater.* **2009**, *19*, 653−661.
(9) Chwieroth, B.; Patton, B.; Wang, Y. *J. Electroceram.* **2001**, *6*, 27−41.
(10) Cho, N. G.; Woo, H.-S.; Lee, J.-H.; Kim, I.-D. *Chem. Commun.* **2011**, *47*, 11300−11302.
(11) Choi, J.-K.; Hwang, I.-S.; Kim, S.-J.; Park, J.-S.; Park, S.-S.; Jeong, U.; Kang, Y. C.; Lee, J.-H. *Sens. Actuators, B* **2010**, *150*, 191−199.
(12) Skála, T.; Veltruská, K.; Moroseac, M.; Matolínová, I.; Cirera, A.; Matolín, V. r. *Surf. Sci.* **2004**, *566−568* (Part 2), 1217−1221.
(13) Wei, B. Y.; Hsu, M. C.; Su, P. G.; Lin, H. M.; Wu, R. J.; Lai, H. J. *Sens. Actuators, B* **2004**, *101*, 81−89.
(14) Zhu, G.; Xi, C.; Xu, H.; Zheng, D.; Liu, Y.; Xu, X.; Shen, X. *RSC Adv.* **2012**, *2*, 4236−4241.
(15) Dirksen, J. A.; Duval, K.; Ring, T. A. *Sens. Actuators, B* **2001**, *80*, 106−115.
(16) Bognitzki, M.; Czado, W.; Frese, T.; Schaper, A.; Hellwig, M.; Steinhart, M.; Greiner, A.; Wendorff, J. H. *Adv. Mater.* **2001**, *13*, 70−72.
(17) Zhang, J.; Fu, J.; Li, F.; Xie, E.; Xue, D.; Mellors, N. J.; Peng, Y. *ACS Nano* **2012**, *6*, 2273−2280.
(18) Dong, Z.; Kennedy, S. J.; Wu, Y. *J. Power Sources* **2011**, *196*, 4886−4904.

(19) Fu, J.; Zhang, J.; Peng, Y.; Zhao, J.; Tan, G.; Mellors, N. J.; Xie, E.; Han, W. *Nanoscale* **2012**, *4*, 3932−3936.
(20) Tiemann, M. *Chem.—Eur. J.* **2007**, *13*, 8376−8388.
(21) Yamazoe, N.; Kurokawa, Y.; Seiyama, T. *Sens. Actuators* **1983**, *4*, 283−289.
(22) Schweizer-Berberich, M.; Zheng, J. G.; Weimar, U.; Göpel, W.; Bârsan, N.; Pentia, E.; Tomescu, A. *Sens. Actuators, B* **1996**, *31*, 71−75.